Leaky RyR2 channels unleash a brainstem spreading depolarization mechanism of sudden cardiac death

Isamu Aiba[a], Xander H. T. Wehrens[b,c,d,e], and Jeffrey L. Noebels[a,f,g,1]

[a]Department of Neurology, Baylor College of Medicine, Houston, TX 77030; [b]Cardiovascular Research Institute, Baylor College of Medicine, Houston, TX 77030; [c]Department of Molecular Physiology and Biophysics, Baylor College of Medicine, Houston, TX 77030; [d]Department of Medicine (Cardiology), Baylor College of Medicine, Houston, TX 77030; [e]Department of Pediatrics, Baylor College of Medicine, Houston, TX 77030; [f]Department of Neuroscience, Baylor College of Medicine, Houston, TX 77030; and [g]Department of Molecular and Human Genetics, Baylor College of Medicine, Houston, TX 77030

Edited by Hee-Sup Shin, Institute for Basic Science, Daejeon, Republic of Korea, and approved June 27, 2016 (received for review March 31, 2016)

Cardiorespiratory failure is the most common cause of sudden unexplained death in epilepsy (SUDEP). Genetic autopsies have detected "leaky" gain-of-function mutations in the ryanodine receptor-2 (RyR2) gene in both SUDEP and sudden cardiac death cases linked to catecholaminergic polymorphic ventricular tachycardia that feature lethal cardiac arrhythmias without structural abnormality. Here we find that a human leaky RyR2 mutation, R176Q (RQ), alters neurotransmitter release probability in mice and significantly lowers the threshold for spreading depolarization (SD) in dorsal medulla, leading to cardiorespiratory collapse. Rare episodes of sinus bradycardia, spontaneous seizure, and sudden death were detected in RQ/+ mutant mice in vivo; however, when provoked, cortical seizures frequently led to apneas, brainstem SD, cardiorespiratory failure, and death. In vitro studies revealed that the RQ mutation selectively strengthened excitatory, but not inhibitory, synapses and facilitated SD in both the neocortex as well as brainstem dorsal medulla autonomic microcircuits. These data link defects in neuronal intracellular calcium homeostasis to the vulnerability of central autonomic brainstem pathways to hypoxic stress and implicate brainstem SD as a previously unrecognized site and mechanism contributing to premature death in individuals with leaky RYR2 mutations.

sudden unexpected death in epilepsy | SUDEP | catecholaminergic polymorphic ventricular tachycardia | CPVT | ryanodine receptor

Up to 10% of individuals with seizures of unknown cause and without known structural cardiac pathology die of sudden unexpected death in epilepsy (SUDEP), and this morbidity is second only to stroke in the number of life-years lost (1). Despite the high mortality rate, comparable to that of sudden infant death syndrome (SIDS), the exact causes are unclear, and there is no effective prediction or intervention. Cardiorespiratory dysfunction and collapse have been observed following generalized tonic–clonic seizures in a small number of monitored cases (2), "near SUDEP" cases (3), and mouse SUDEP models (4–6). Genes linked with the most common cardiac LQT syndromes including LQT1 (KCNQ1), LQT2 (KCNH2/HERG), and LQT3 (SCN5A) are expressed in both the human heart and brain, where mutations in the kinetics of these membrane ion channels prolong depolarization and produce combined seizure, cardiac arrhythmia, and sudden death phenotypes (7, 8). Because mutations in these ion channel genes currently explain only a small fraction of SUDEP cases (7), the search for additional genes and mechanisms is a high priority to understand and treat sudden death risk.

Along with cardiac arrhythmia, recent findings in voltage-gated ion channelopathy models point to an extracardiac, central autonomic involvement of these genes in the events leading to sudden cardiac death. Spreading depolarization (SD) is a slow propagating wave of cellular depolarization that occurs in human brain and is known to contribute to transient neurological deficits during migraine auras (9, 10). Once triggered, the profound local depolarization of neurons and glia compromises electrical brain activity and energy metabolism. We recently reported that cortical seizures lead to ictal hypoxia and SD in mouse SUDEP models, resulting in cortical electroencephalography (EEG) depression and terminal cardiorespiratory arrest (11). We also found that slices of dorsal medulla from these Kv1.1- and Nav1.1-deficient SUDEP mice facilitated SD generation in vitro following hypoxic challenge. These results suggest that gene mutations that lower SD threshold may increase the risk of sudden death via peri-ictal hypoxic depolarization of brainstem cardiorespiratory control centers, implicating a site for therapeutic intervention.

The basis for the complex loss of homeostasis in the neuronal microenvironment during SD involves aberrant, regenerative glutamate transmitter release and extracellular potassium accumulation, but its molecular triggering mechanisms remain poorly understood. The first and one of the most studied SD-related genes is a gain-of-function mutation in *CACNA1A* encoding the P/Q-type calcium channel, originally identified in familial hemiplegic migraine (FHM1) (12). Mice carrying these mutations show increased high voltage-activated calcium current, resulting in facilitated transmitter release at excitatory synapses, lower SD threshold, faster SD propagation, seizures, and early lethality (13–15). In contrast, mice with loss-of-function P/Q channel mutations show an increased SD threshold and normal lifespan (16). Although these studies underscore the critical role of plasmalemmal presynaptic calcium channels in the generation of SD and sudden death, the roles of genes regulating intracellular Ca^{2+} levels that may also influence transmitter release remain unknown. The ryanodine receptor-2 (RyR2) is an intracellular Ca^{2+} channel that elevates cytoplasmic Ca^{2+} by release from endo- and sarcoplasmic stores upon activation (17). Among the three isoforms (RyR1–3), RyR2 is critical for cardiac excitation–contraction, and gain-of-function "leaky" mutations are found in patients with catecholaminergic

Significance

Gain-of-function "leaky" ryanodine receptor-2 (RyR2) mutations are detected in many cases of human sudden cardiac death and sudden unexpected death in epilepsy. The early lethality is considered to be due to arrhythmogenic behavior of cardiomyocytes caused by excess intracellular calcium ions released from internal stores. In this study, we find that the leaky RyR2 mutation also modulates neurotransmitter release from neurons in brainstem autonomic centers and facilitates spreading depolarization, which when provoked silences autonomic microcircuitry in the dorsal medulla. When seizures were generated in mice carrying a leaky RyR2 mutation, the mice experienced sudden cardiorespiratory collapse concomitant with brainstem spreading depolarization. These findings indicate that in addition to the myocardium, the brainstem is a target of leaky RyR2 mutations.

Author contributions: I.A. and J.L.N. designed research; I.A. performed research; I.A. analyzed data; and I.A., X.H.T.W., and J.L.N. wrote the paper.

The authors declare no conflict of interest.

This article is a PNAS Direct Submission.

[1]To whom correspondence should be addressed. Email: jnoebels@bcm.edu.

This article contains supporting information online at www.pnas.org/lookup/suppl/doi:10.1073/pnas.1605216113/-/DCSupplemental.

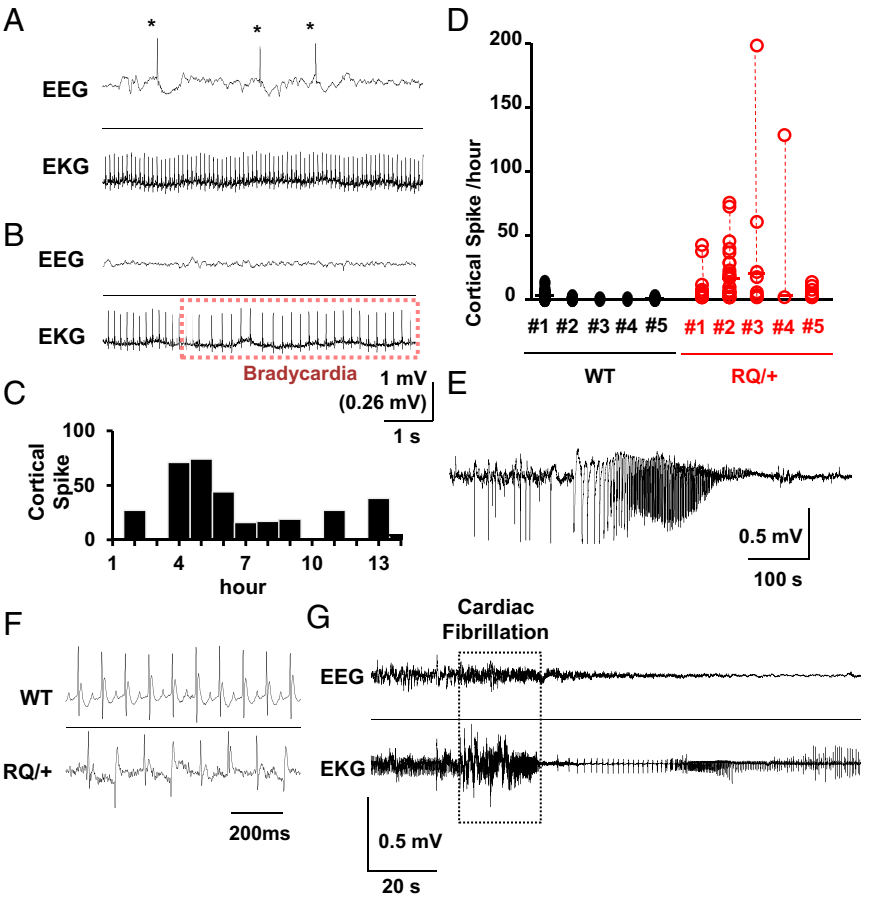

Fig. 1. In vivo simultaneous EEG and EKG monitoring of awake RQ (R176Q/+) mutant and WT male mice (P30–50, $n = 5$ each) revealed resting abnormalities in brain and cardiac rhythms. (*A* and *B*) Representative traces of cortical spikes (*) with normal EKG (*A*) and a brief episode of bradycardia with normal EEG activity (*B*). (*C*) Histogram of spike distribution from a RQ mouse showing the large variability in EEG spike occurrence. (*D*) Summary of spike frequency from five RQ mutant and WT animals. Each data point shows numbers of spikes in 1-h bins. (*E*) EEG tracing showing an example of a spontaneous convulsive seizure in a RQ mutant mouse. (*F*) EKG recordings from WT (*Top*) and RQ mutant mice (*Bottom*) 10 min after caffeine injection (100 mg/kg, i.p.). Cardiac arrhythmias were seen in RQ mutant but not WT mice. (*G*) Caffeine injection led to cardiac fibrillation and arrest in RQ mutant mice. No abnormal EEG discharges were seen during caffeine-induced lethal cardiac arrhythmias.

polymorphic ventricular tachycardia (CPVT) (18, 19) linked to sudden death without structural cardiac abnormality (20, 21). Leaky RyR2 mutations generate intrinsic cardiac instability commonly assumed to explain cardiac arrest, but these patients also experience sinus bradycardia (22), suggestive of abnormal regulation of premotor vagal nerve excitability. It is unknown whether they might also contribute to premature death by lowering the threshold for hypoxic depolarization that silences brainstem cardiorespiratory pace-making circuitry. RyR2 is also expressed in the central nervous system (23) and contributes to vesicular transmitter release (24–26) and postsynaptic dendritic spine function (27). A gain-of-function or leaky RyR2 mutation (R2474S) lowered the threshold for seizures in mouse brain (28), and other missense RyR2 mutations have been detected in SUDEP victims, of which two (Q2958R and C1489R) are linked to CPVT (7, 29, 30).

Here we examined whether abnormal intracellular Ca^{2+} homeostasis due to a leaky RyR2 mutation can modify synaptic transmission, network excitability, and the SD threshold in knock-in mice carrying the RyR2 R176Q (hereafter RQ), a gain-of-function mutation identified in a CPVT patient (31). Our study demonstrates that this mutation is associated with selective synaptic transmission changes in excitatory cortical and vagal motor neurons and network hyperexcitability and significantly lowers cortical and brainstem SD thresholds. Cortical seizures in the RQ mutant mouse trigger SD and cardiorespiratory arrest associated with bradycardia, identifying a brainstem central autonomic pathway mechanism underlying leaky RYR2 sudden death risk and validating the inclusion of RYR2 as a SUDEP risk gene in clinical exome profiling.

Results

In Vivo Characterization of Cortical Spikes, Seizure, and SD in RYR2 RQ Mutant Mice. We first characterized the cortical excitability phenotype of awake RYR2 R176Q (R176Q/+) knock-in (hereafter RQ) mice by video EEG–electrocardiography (EKG) recordings in unanesthetized freely moving mice. Prolonged EEG–EKG monitoring revealed spontaneous bilateral cortical epileptiform spike discharges in RQ mutant mice (Fig. 1 *A* and *B*). Abnormal spike discharges were mostly absent when mice were behaviorally active and increased at rest. Spectral EEG analysis revealed that cortical theta power (4–7 Hz), typically prominent during drowsiness, was significantly increased ($200.1 \pm 71.4\%$ of spike-free period, $n = 5$, $P < 0.05$) during spike-frequent periods compared with spike-free periods, although there was large daily variability (Fig. 1 *C* and *D*). Seizure activity was rare, and only one spontaneous seizure was detected in one out of five mutant mice during 16–48 h of monitoring in each mouse (Fig. 1*E*). Spontaneous episodes of bradycardia and artrioventricular (AV) block were detected in three out of five RQ mice, however these cardiac events did not associate temporally with abnormal EEG activity (Fig. 1*B*). Similar episodes of sinus bradycardia have been reported in CPVT patients with RyR2 mutations (22).

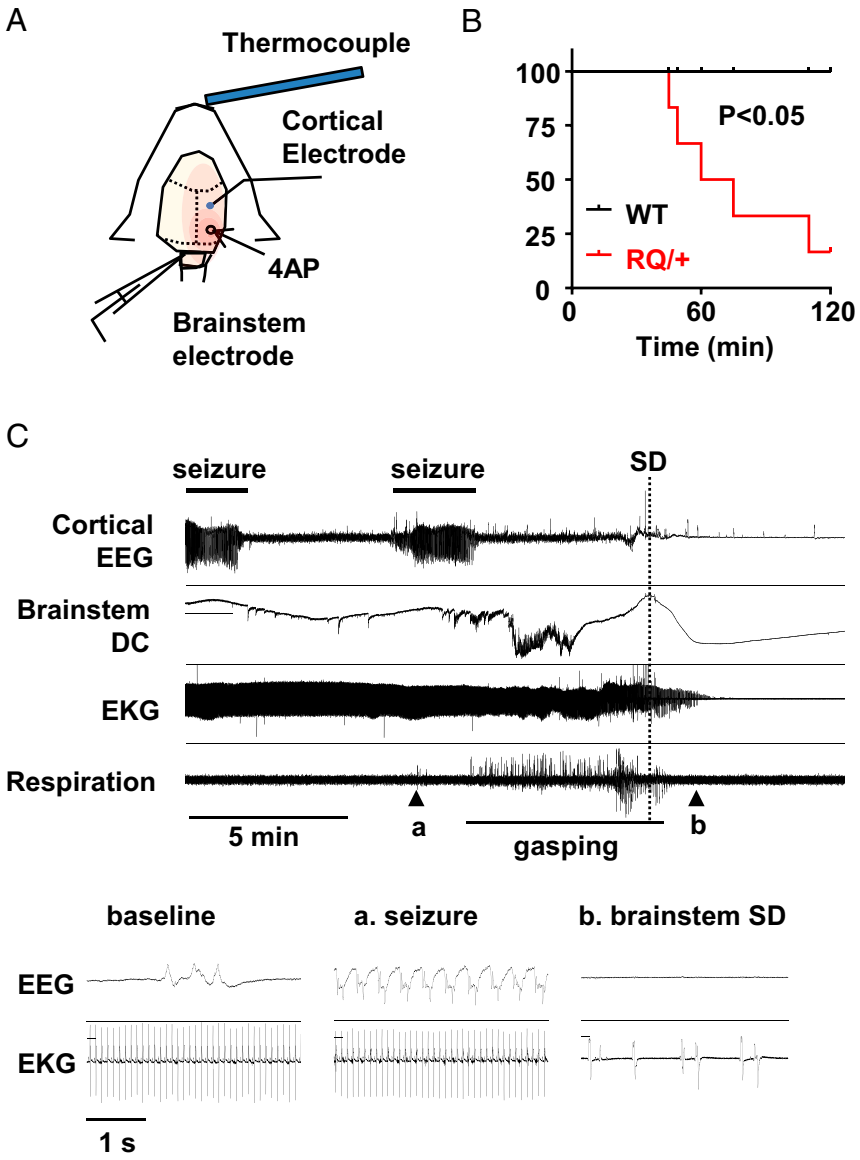

Fig. 2. Seizure monitoring in vivo. (*A*) Experimental procedure. Juvenile mice (P18–25) were lightly anesthetized with urethane, and body temperature was maintained at 37 °C. Cortical EEG was recorded from an Ag/AgCl electrode implanted on the skull over the somatosensory cortex. Seizures were evoked by topical application of 4AP (100 mM). Heart rate was monitored with s.c. electrodes implanted on the thoracic wall. (*B*) Plot of survival rate following 4AP application. Seventy-one percent of RQ mutant mice (5 of 7) died shortly after 4AP-induced seizure, whereas none (0 of 7) of the WT mice died. (*C*) Representative recording showing terminal brainstem SD and cardiac arrhythmias following recurrent cortical seizures. *Insets* show EEG/EKG activity during baseline, during seizure (*a*), and after brainstem SD (*b*).

We next examined the effect of the RyR2 agonist, caffeine. Similar to isoproterenol challenge (21), i.p. injection of caffeine at a high dose (100 mg/kg) promptly resulted in abnormal EKG patterns in RQ mutant mice characterized by frequent bigeminy and sporadic ventricular fibrillation (Fig. 1 *F* and *G*). At the onset of cardiac fibrillation, the EEG showed low-amplitude, high-frequency activity. In WT mice, caffeine evoked only a brief period of tachycardia that resolved within 5 min without EEG abnormalities. All injected RQ mutant mice died within 2 h postinjection, whereas none of the WT mice died following the same treatment. Collectively these data indicate that the RyR2 RQ mutation increased cortical excitability and facilitated caffeine-induced lethal cardiac arrhythmias.

High Incidence of Seizure-Induced Death in RQ Mutant Mice. We tested the vulnerability of juvenile RQ mice to seizure-induced death. Under light urethane anesthesia, cortical seizures were evoked in vivo by topical application of a pledget soaked in the convulsant potassium channel blocker 4-aminopyridine (4AP; 100 mM) while simultaneously monitoring cortical EEG, brainstem direct current (DC) activity and the electrocardiogram (Fig. 2*A*). In both control and RQ mutant mice, EEG seizures were detected ~40 min after 4AP application. During 2-h recording sessions, five of seven RQ mutant mice (71%) died shortly following the appearance of recurrent seizures, whereas all WT mice survived (Fig. 2*B*; $P = 0.025$, Mantel–Cox test). Death (defined by the termination of heartbeat and respiration) followed minutes after the onset of SD in the dorsal medulla. An example is shown in Fig. 2*C*. In this recording, lethal cardiac arrhythmias occurred >5 min after the last seizure. Recordings from the dorsal medulla surface detected postictal abnormal excitation overriding a strong depolarizing negative DC potential that was associated with the onset of agonal breathing and

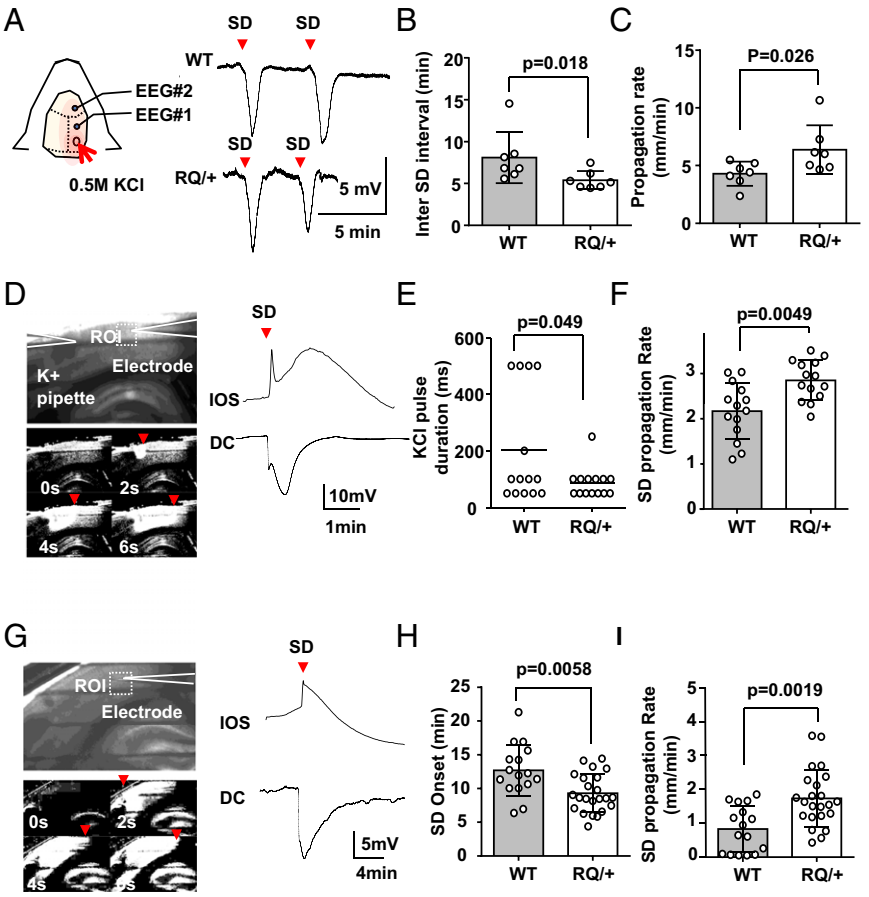

Fig. 3. In vivo and in vitro characterization of SD thresholds. (*A–C*) Characterization of cortical SD frequency in vivo. SD was evoked by topical application of KCl-soaked gelfoam in the cranial window and was detected with a pair of Ag/AgCl electrodes. (*A*) Traces show representative DC recordings from WT (*Top*) and RQ mutant (*Bottom*). The inter-SD interval was significantly shorter (*B*) and the propagation rate was faster (*C*) in the RQ mutant cortex. (*D–F*) Characterization of KCl-evoked cortical SD in vitro. SD was evoked by local microinjection of 1 M KCl and detected by DC recording and IOS change (*D*). Raw image (*Top*) and a sequence of ratio images showing bright region of IOS change of SD (*Bottom*). The effective KCl pulse duration needed to trigger SD was shorter (*E*) and the SD propagation rate was faster (*F*) in cortical slices obtained from the RQ mouse. For each genotype, 14 slices from four adult mice were used. (*G–I*) Characterization of cortical SD evoked by OGD. SD was evoked by continuous exposure to OGD solution (0% O_2 and 2 mM glucose). The latency to SD onset was shorter (*H*) and the propagation rate was faster (*I*) in slices from RQ mutant mice. WT, 16 slices from 4 mice; RQ, 23 slices from 5 mice. Bar graph, mean ± standard deviation.

eventually led to a second terminal brainstem SD in the mouse (Fig. 2*C*). As seen previously in other SUDEP mouse models (11), the onset of the cardiac arrhythmias occurred within 1 min after the brainstem SD event. Although the lack of systemic physiological monitoring of oxygen saturation and blood pressure during these recordings is a potential caveat, these results indicate that the RQ mouse is highly susceptible to seizure-induced lethality, likely due to hypoxia/hypoxemia resulting from peri-ictal cardiorespiratory instability and a lower threshold for SD within the central autonomic microcircuitry.

Lower Threshold of Cortical SD in Intact and Isolated RQ Mutant Mouse Brain. We directly examined whether the SD threshold is lower in RQ mutant mouse brain using three independent methods of triggering this event. The SD threshold was first characterized in adult RQ mutant mouse cortex in vivo. Cortical SD events were evoked in lightly urethane-anesthetized mouse cortex by topical application of a pledget soaked in 0.5 M KCl, and DC recordings were made in the first hour from a pair of silver surface electrodes. RQ mutant mice showed a significantly shorter interevent interval of spontaneous recurrent SD waves compared with WT control mice (WT, 8.1 ± 3.0 min; RQ, 5.4 ± 1.1 min; $n = 7$, $P = 0.018$), indicating a lower regenerative SD threshold (Fig. 3*B*). Accordingly, SD frequency was also increased in the RQ mouse cortex (WT, 7.5 ± 1.8 SD per hour; RQ, 10.4 ± 2.0 SD per hour; $P = 0.016$). The propagation velocity of the SD wave front was also increased in the mutant cortex to 148% of control value (WT, 4.3 ± 1.1 mm/min; RQ, 6.4 ± 2.1 mm/min; $n = 7$ each, $P = 0.026$) (Fig. 3*C*).

The potassium-evoked cortical SD threshold was also examined ex vivo in acutely prepared somatosensory cortical slices maintained in vitro. SD was evoked by repeated focal pressure microinjection of KCl (1 M, 30 psi) in layer II/III, and the ejection pulse was incrementally prolonged until an SD was triggered. SD was optically detected in slices by a change in light transmission (intrinsic optical signal, IOS) that is associated with a large negative DC potential shift (Fig. 3 *D* and *G*). The traveling IOS in layer II/III typically preceded the IOS spreading across other cortical layers, as described in an earlier study (32). The duration of extracellular KCl pulses required for SD generation was somewhat shorter (42% of control) in the mutant than in WT control slices (WT, 204 ± 200 ms; RQ, 86 ± 53 ms; $n = 14$, $P = 0.049$; Fig. 3*E*). The propagation velocity of KCl-evoked SDs was also significantly increased in RQ mice (138% of control; WT, 2.9 ± 0.8 mm/min; RQ, 3.8 ± 0.6 mm/min; $n = 14$, $P = 0.0049$) (Fig. 3*F*).

Cortical SD was also characterized in an oxygen/glucose deprivation (OGD) model (95% N_2 and glucose 5 mM). Exposure to OGD bath solutions reliably triggered SD in all RQ mutant slices, whereas SD either did not occur or propagation was extremely slow in 38% (6 of 16) of WT slices. The latency to OGD SD appearance was

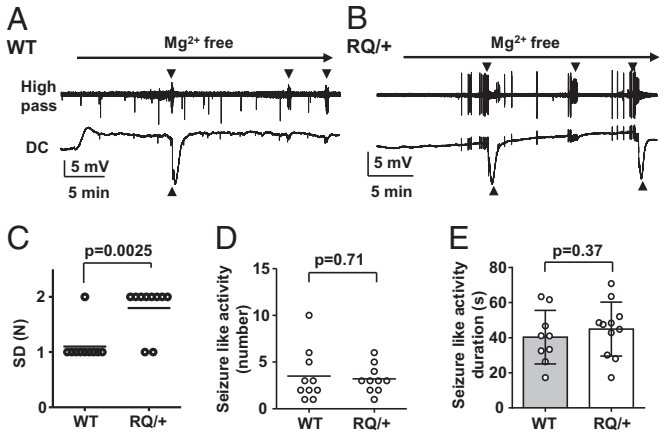

Fig. 4. Characterization of seizure-like activities and SD in vitro. Representative traces from WT (*A*) and RQ mutant cortical slices (*B*) exposed to Mg^{2+}-free ACSF solution. High pass-filtered recording (*Top*) and DC components (*Bottom*) from the same recordings are presented. Arrowheads indicate spontaneous seizure-like activity (*Top*) and SD (*Bottom*). The number of SD events was greater in RQ mutant than +/+ slices (*C*), whereas the numbers (*D*) and durations (*E*) of seizure events were not different. For each genotype, 10 slices from 3 mice were used. Bar graph, mean ± standard deviation.

significantly shorter (WT, 9.7 ± 3.8 mm/min; RQ, 6.3 ± 2.8 mm/min; $n = 16$ and 23, respectively, $P = 0.0058$), and the propagation velocity was faster in RQ slices (WT, 2.5 ± 2.1 mm/min; RQ, 5.3 ± 2.5 mm/min; $n = 16$ and 23, respectively, $P = 0.0019$) (Fig. 3 *H* and *I*).

Lastly, we examined SD threshold dynamics using a third method by superfusing slices with nominally Mg^{2+}-free solution. Exposure to Mg^{2+}-free solution triggered waves of SD preceded in all cases by brief seizure-like activity (Fig. 4 *A* and *B*). Consistent with the other two models, the number of recurrent SD events was significantly increased in RQ mutant mice (Fig. 4*C*). On the other hand, the number and duration of seizure-like discharges were not different between WT and RQ slices (Fig. 4 *D* and *E*). Taken together, these data provide consistent evidence that the leaky RyR2 mutation significantly facilitates SD generation in mouse cortex without a large effect on the fast epileptiform synchronization in Mg^{2+}-free cortical synaptic networks.

Increased Excitatory Postsynaptic Currents in Leaky RyR2 Layer II/III Neurons. To further characterize these findings at the cellular level, we measured the intrinsic membrane excitability of RQ cortical neurons in vitro. Layer II/III neurons were chosen because SD preferentially propagates in superficial rather than deeper cortical layers, and RyR2 mRNA expression in neocortex is highest in these neurons (Allan Mouse Brain Atlas). Whole-cell recordings were made from visually identified pyramidal neurons, and their intrinsic excitability was determined. We detected a significant increase in the slow after-hyperpolarization (AHP) following an evoked action potential train in mutant versus WT neurons (Fig. 5 *A* and *E*), a parameter known to be sensitive to RyR inhibition (33). However, we found no differences in resting membrane potential, resistance, or action potential frequency to injected depolarizing currents in these cells (Fig. 5 *B*–*D*). These data suggest that intrinsic neuronal excitability per se is unlikely to contribute to the lowered SD threshold and abnormal cortical EEG in the RQ mutant.

We next examined synaptic events in these layers. Layer II/III pyramidal neurons were voltage clamped at –70 mV to detect spontaneous excitatory postsynaptic currents (sEPSCs). The RQ mutation did not affect sEPSC frequency (WT, 10.9 ± 5.0 Hz; RQ, 12.6 ± 5.2 Hz; $P = 0.33$, $n = 16$ each) or amplitude (WT, 8.2 ± 3.3 pA; RQ, 7.8 ± 1.9 pA; $P = 0.74$, $n = 16$). However, significant differences in synaptic release were seen when miniature (mEPSC) synaptic events were isolated by 1 μM TTX added to the bath solution. In these experiments, the mean mEPSC amplitude was significantly larger (125% of control) in RQ mutant mice compared with WT control cells (Fig. 6 *A*, *C*, and *D*). Mean mEPSC frequency did not differ between genotypes (Fig. 6*B*). We also characterized inhibitory postsynaptic currents (IPSCs) from the same neurons by voltage-clamp recording at 0 mV. Similar to sEPSCs, the sIPSCs did not show any differences in mean frequency (WT, 11.8 ± 4.6 Hz; RQ, 15.3 ± 7.6 Hz; $P = 0.13$, $n = 12$ and 18, respectively). Unlike the mEPSCs, no differences were seen in the mean amplitudes of mutant mIPSCs (WT, 10.2 ± 2.4 pA; RQ, 10.7 ± 4.1 pA; $P = 0.13$, $n = 12$ and 18, respectively; Fig. 6 *E*–*H*). These results indicate a selective facilitating effect of leaky RYR2 on cortical excitatory synapses with a change in excitatory–inhibitory balance at the synaptic level, shifting the network toward increased excitability in the RQ mutant.

The mutant RQ effect on excitatory synaptic transmission was further characterized by examining the paired pulse ratio (PPR), a measure of residual presynaptic intracellular calcium level, of evoked EPSCs triggered by bipolar stimulation of cortical layer IV. In RQ mutant pyramidal neurons, PPR was significantly reduced and less variable than in WT neurons (ratio of P2/P1; WT, 1.35 ± 0.43; RQ, 0.97 ± 0.18; $n = 12$ and 18, respectively; Fig. 7 *A* and *B*). There was an outlier in the WT, which did not affect the

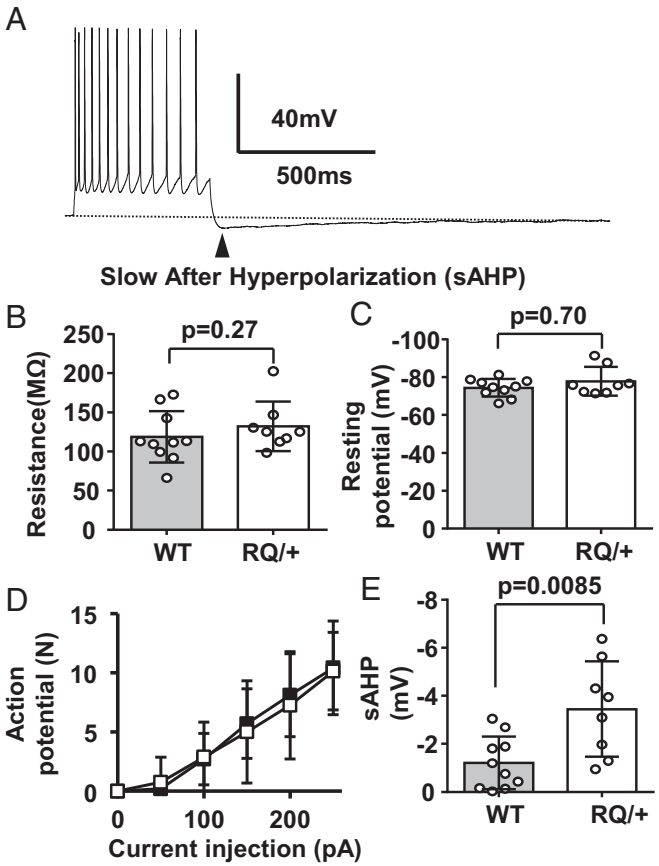

Fig. 5. Intrinsic excitability of layer II/III pyramidal neurons from the somatosensory cortex was unchanged. (*A*) Representative trace showing action potentials evoked by a rectangular pulse (+200 pA, 500 ms) and consequently slow AHP. There were no differences in input resistance (*B*), resting potential (*C*), or the number of evoked action potentials by a series of current injections (50 pA increment) (*D*). The maximal amplitude of the slow phase of AHP (sAHP) was significantly larger in RQ mutant than +/+ neurons (*E*). Ten and eight slices from three WT and RQ mice were used. All graphs, mean ± standard deviation.

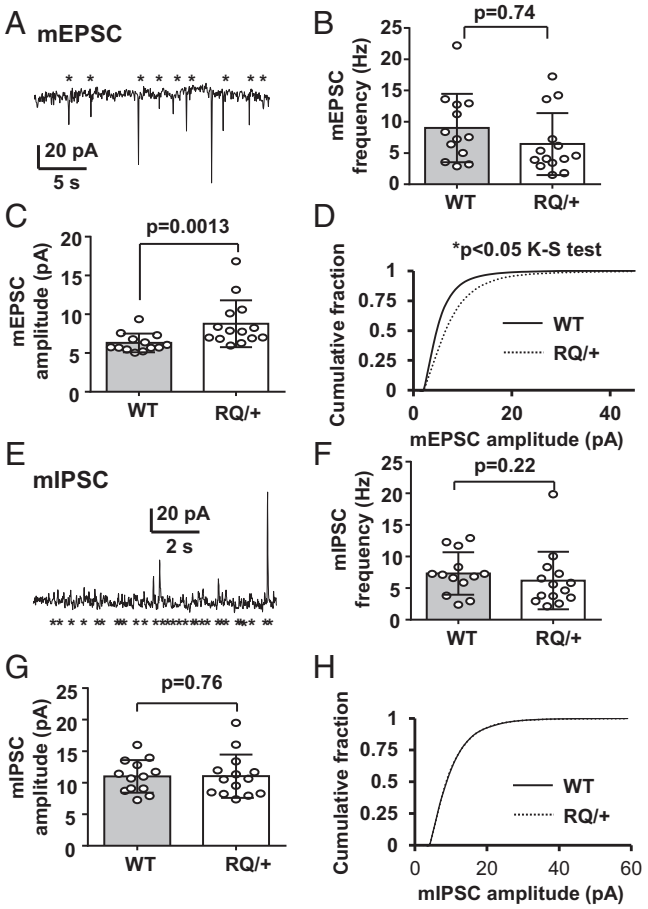

Fig. 6. Characterization of mEPSCs and miniature IPSCs (mIPSCs) recorded in vitro from layer II/III pyramidal neurons in slices from the somatosensory cortex. (*A*) Representative trace of mEPSCs. An asterisk indicates a detected event. (*B*) There was no genotypic difference in mEPSC frequency, however in *C* the mean mEPSC amplitude was significantly larger in the RQ mutant. (*D*) Mean cumulative histogram of mEPSC amplitude distribution from WT and RQ mutant mice ($P < 0.05$, Kolmogorov–Smirnov test). (*E*) Representative trace of mIPSC recording. There were no differences in mean IPSC frequency (*F*) or amplitude (*G*). (*H*) Mean cumulative histogram of mIPSC amplitudes shows no difference in the distribution between genotypes. WT, 13 neurons from three mice; RQ, 14 neurons from three mice. Bar graph, mean ± standard deviation.

significance level. This result suggests an increased probability of evoked presynaptic glutamate release due to leaky ryanodine receptors at excitatory mutant synapses. These results collectively indicate that the leaky RyR2 mutation selectively strengthens release at excitatory synapses in layer II/III neurons, contributing to enhanced excitability of RQ mutant cortical networks.

RQ Mutation Reduces the Threshold for Brainstem SD and Postictal Survival in RyR2 Mutant Mice. We next examined whether the leaky RyR2 mutation also modifies SD threshold in cardiorespiratory control regions of brainstem slices prepared from juvenile WT and RQ mice. SD was triggered by exposure to OGD solution (0% O_2/5 mM glucose) and was detected in both genotypes as a slow propagating wave of enhanced IOS in these slices (Fig. 8 *A* and *B* and Movie S1). The enhanced IOS signal always appeared first along the lateral margins of the nucleus tractus solitarius (NTS) and subsequently invaded throughout the dorsal vagal nuclear complex. The mean latencies to SD generation following OGD exposure, an indirect measure of SD threshold, were significantly shorter in slices prepared from RQ mice than control (55% of control; WT, 8.7 ± 3.3 min; RQ, 4.9 ± 1.6 min; $n = 11$ and 14 respectively; $P = 0.001$; Fig. 8*C*).

Excitatory synapses of dorsal motor vagal (DMV) neurons were also characterized (Fig. 8 *D–F*). Similar to cortical pyramidal neurons, mEPSC amplitude was significantly increased in the RQ mutant mice (34% increase; WT, 12.5 ± 4.3 Hz; RQ, 16.8 ± 4.0 Hz; $n = 18$, $P = 0.004$), whereas the mean frequency was unchanged (WT, 7.1 ± 5.8 Hz; RQ, 7.2 ± 4.8 Hz; $n = 18$, $P = 0.96$). Similar experiments were performed in the NTS, however basal synaptic release events were highly variable between recorded cells and were not further analyzed.

These in vitro results indicate that the leaky RyR2 mutation contributes to a lower SD threshold in cardioregulatory brainstem microcircuitry and that the central autonomic system in this mutant mouse is more vulnerable to hypoxic stress. Elevated release at excitatory synapses in the dorsal vagal complex also likely contributed to episodes of spontaneous bradycardia and seizure-induced death in RQ mutants (Figs. 1 and 2).

Discussion

The major translational finding of this study is that a human leaky RyR2 mutation found in cardiac disease and SUDEP cases lowers SD threshold in the brain and increases susceptibility to seizure-induced death in a knock-in mouse model, strongly implicating a brainstem central autonomic mechanism contributing to what has been considered primary myocardial failure and sudden death in human cases bearing this cardiac arrhythmia mutation. Over 150 RyR2 mutations have been identified in human CPVT1 cases, one of several calcium channelopathies underlying cardiac arrhythmias (34). We evaluated the RQ model for the presence of an epileptic phenotype, as epilepsy is an independent risk factor for sudden cardiac death (35, 36). We found that mice bearing this mutation had strong evidence of cortical hyperexcitability in the form of frequent interictal cortical EEG spike discharges, a neurophysiological biomarker of epilepsy. Spontaneous seizures, although detected, were rare in this model, possibly owing to the enhancement of membrane AHP detected in excitatory neurons, which serves as a brake for recurrent discharge activity and aberrant fast cortical synchronization. If present in humans, this feature may explain the relative lack of an epilepsy phenotype in clinical cases of leaky RYR2 identified with syncopy and other cardiac manifestations. Nevertheless, high-resolution genomic analyses are beginning to reveal abnormalities in genomic architectures of epilepsy and SUDEP victims, including mutations in *RYR2* (29), and leaky RYR mutations are common to both clinical populations. Because SD also contributes to the pathophysiology of other neurological disorders, including migraine with aura and delayed

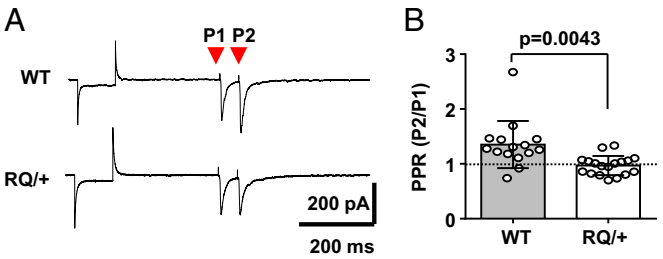

Fig. 7. Enhanced evoked presynaptic release properties at RQ cortical synapses. Shown is the PPR of evoked EPSCs in layer II/III pyramidal neurons from the somatosensory cortex. Pairs of evoked EPSCs (100 ms interpulse interval) were triggered following a membrane seal test. Representative traces (*A*) and bar graphs are shown (*B*). PPR was significantly smaller in the RQ mutant than in WT control neurons, suggesting that presynaptic glutamate initial release probability is increased at RQ mutant synapses. WT, 14 neurons from 4 mice; RQ, 18 neurons from 5 mice. Bar graph, mean ± standard deviation.

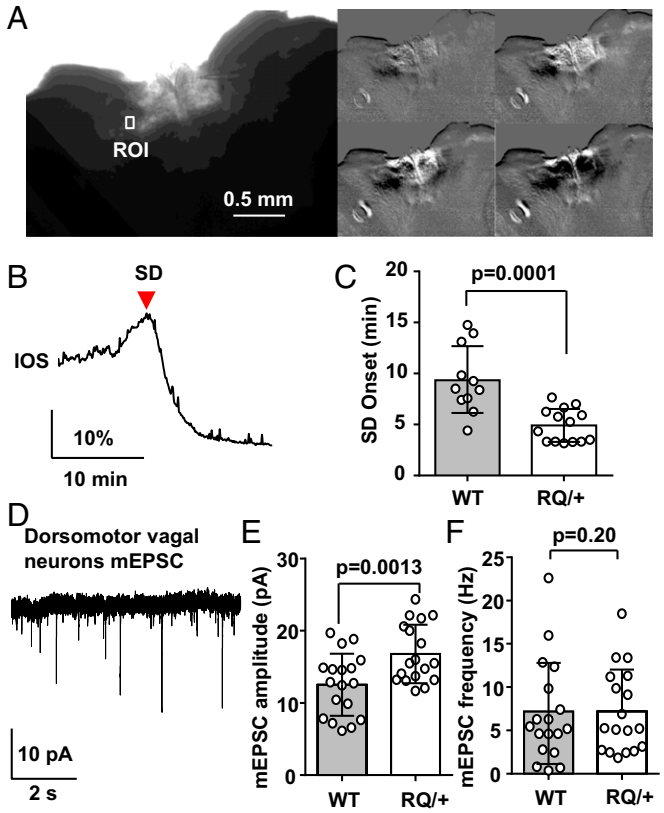

Fig. 8. Lowered SD threshold in dorsal vagal complex of the RQ mutant brainstem. (*A–C*) Characterization of SD generated in dorsal medulla in vitro. Brainstem slices containing the dorsal vagal complex were exposed to OGD solution (0% O_2, 5 mM glucose), and SD was detected by monitoring intrinsic light transmission signals in the region of interest (ROI) positioned in the lateral NTS (*A* and *B*). A raw image of an acute brainstem slice (*Left* large) and a sequence of ratio images showing spreading light transmission changes following OGD exposure (*Right*). The latency to SD onset was significantly shorter in the RQ mutant (*C*). WT, 11 slices from 4 mice; RQ, 15 slices from 5 mice. (*D–F*) Characterization of mEPSC in dorsomotor vagal (DMV) neurons. (*D*) Representative trace of mEPSCs recorded from a DMV neuron. The mean amplitude was significantly larger in RQ mutant neurons (*E*), whereas the mean frequency did not differ (*F*). WT, 18 neurons from 4 mice; RQ, 18 neurons from 4 mice. Bar graph, mean ± standard deviation.

progression of ischemic brain injury (10, 37), the presence of leaky RyR2 mutations may also contribute to the neurological consequences of related cerebrovascular disorders.

Variable Severity of Calcium Homeostasis Phenotype in Mouse SUDEP Models. SD and calcium homeostasis have been extensively studied in voltage-gated P/Q-type Ca^{2+} channel mutations, where a gain-of-function results in a several-fold decrease in cortical SD threshold. The degree of facilitation of the SD phenotype in RQ mutants detected here is somewhat smaller than that found in one of the PQ channel mutants, R192Q, where SD propagation was greatly enhanced and SD propagated into subcortical structures (38). These mutant mice also had spontaneous seizures and shorter survival than the RQ mutant mice studied here. The variance may reflect the different roles of these genes in calcium ion homeostasis and may also depend on the specific mutations and the inbred genetic backgrounds studied. Over 150 *RYR2* gene polymorphisms have been linked to CPVT (34, 39), and the severity of the human arrhythmias differs. The phenotype of the RQ mutant mice studied here shows a milder cortical excitability phenotype than that identified in a different leaky mutation (R2474S) from a CPVT patient; that mutant mouse showed spontaneous cortical seizures, unlike most RQ mutants in the present study (28). The clinical phenotypic spectrum is also broad, and in one human study cohort, leaky RyR2 mutations were detected in 15% of fully asymptomatic individuals (31).

RQ Mutation Selectively Enhances Excitatory Synaptic Transmission. The RYR2 mechanism operating at excitatory synapses has been previously explored. Calcium-induced calcium release from internal stores contributes to Ca^{2+} transients imaged in hippocampal axon terminals and underlies both spontaneous release and paired-pulse facilitation of EPSPs (40). RQ channels have leaky biophysical properties that increase and prolong Ca^{2+} release from intracellular stores (19), thereby modulating Ca^{2+} handling at presynaptic release sites. The enhanced mEPSC amplitude in the RQ mutant was also consistent with the effects of the RyR2 agonist, caffeine, on the same synapse in WT mice (24). We found that initial release probability at RQ mouse layer II/III excitatory cortical synapses was elevated, as revealed by mEPSC analysis and reduced PPR of evoked EPSCs. The reduction in PPR is somewhat unexpected, as a previous study showed that pharmacological RyR inhibition decreases the amplitude of the second postsynaptic response (40). Because RYR2 inhibition was reported to rescue leaky RYR2-related hyperexcitability when administered chronically (28), this response might be explained by downstream postnatal developmental changes in synaptic plasticity due to early effects the mutation has on intracellular Ca^{2+} homeostasis (41, 42) and will require additional exploration.

We found that SD is significantly potentiated by a leaky RQ ryanodine receptor, and the enhanced excitatory but not inhibitory synaptic transmission likely contributes to this effect. A similar selective enhancement at cortical excitatory but not inhibitory synapses along with a lower SD threshold was noted in the gain-of-function mutation (R192Q) of the P/Q channel calcium gene *Cacna1a* (15). Interestingly, selective sparing of IPSCs was also observed in the P/Q calcium channel mutation model, and one suggestion to explain this selectivity is that release probability is already high in GABAergic nerve terminals, masking further facilitation by the transgene (15). Because RyRs have a significant contribution to release probability (25), this possibility could equally explain the absence of IPSC potentiation in RQ mice.

Additional mechanisms can be considered. Intracellular Ca^{2+} release by RyRs contributes to NMDAR-dependent long-term postsynaptic potentiation (43, 44). Importantly, the postsynaptic Ca^{2+} release by RyRs was seen only during early development (<P20), and the leaky RyR2 may contribute to establishment of abnormal synaptic strength during this critical period. RyRs are also present in astrocytes, and altered glial intracellular calcium signaling might contribute to the SD phenotype of RQ mouse brain (45). Along with synaptic effects, we found that the RQ mutation significantly increased postspike AHP in cortical neurons. In the absence of increased GABA release, enhancement of the late AHP is likely due to increased activation of Ca^{2+}-sensitive potassium (SK) channels (46). Increased neuronal AHP limits repetitive high-frequency firing and might explain why seizures are rare in the RQ mouse. Although the mechanism for this selectivity of excitatory over inhibitory synapses in both mutants is unclear, our study confirms that, regardless of the underlying molecular mechanism, enhanced presynaptic transmitter release due to intracellular calcium elevation at excitatory synapses facilitates SD propagation.

RyR2 Regulates Brainstem Parasympathetic Drive. Most cases of sudden cardiac death in CPVT are considered to be due to ventricular tachycardia/fibrillation driven by sympathetic stimulation (47). Paradoxically, many patients show sinus bradycardia at rest (22, 48–50), and not a small fraction of death is related to AV block and bradycardia (51). The RQ mouse showed this bradycardia phenotype (Fig. 1), and other mouse SUDEP models also exhibit interictal spontaneous bradycardia and postictal death associated with bradycardia (4, 5). In these models, seizure-induced

death could be prevented by the parasympathetic blocker atropine, and the same treatment has also been effective for CPVT mice and human cases (52). Our data indicate that RyR2 facilitates presynaptic glutamate release in central parasympathetic dorsomotor vagal neurons. The involvement of RyR channels in this central autonomic microcircuit was previously demonstrated using RyR modulators to modify the excitability of dorsal premotor vagal neurons (53) and the sensory afferent vagal nerve inputs terminating in the NTS (54, 55). Thus, abnormal hyperexcitability of the central excitatory input to the dorsal vagal brainstem microcircuit may contribute to episodic interictal bradycardia as well as depress cardiac function during seizures. We suggest that, through still unexplained molecular remodeling in the brainstem, the RYR2 defect might also increase susceptibility of the dorsal vagal complex to hypoxic depolarization and sudden death.

The RQ mouse model provides additional evidence supporting the pathophysiological role of a brainstem mechanism contributing to death that has been recently associated with two "epileptic" membrane ion channel gene mutations underlying SUDEP. Although the specific mouse model studied here does not display a severe spontaneous seizure phenotype by itself, the coexistence of leaky RYR2 mutations with other genes that enhance epilepsy or cardiac arrhythmia (29) establish RYR2 as a strong additional genetic candidate for sudden death risk.

Materials and Methods

Animals. All animal research was approved and performed in accordance with Baylor College of Medicine Institutional Animal Care and Use Committee guidelines and regulations.

The R176Q mice were generated as described previously (21) and maintained on the C57BL/6J genetic background. Mice were kept on a 12 h light/dark cycle. Both male and female 4–8-wk-old adult mice were used for the experiments on cortical excitability, and juvenile (P18–P25) mice were used for brainstem studies. The numbers of animals and their ages in each study are described in the figure legends.

Mouse tail clips were digested in Direct PCR reagents (Viagen Biotech), and the lysates were used for genotyping. The genotype was determined by the PCR method using a pair of primers (F, CAAGATGAGATCATCTCCAACTT; R, CACAGGGACTGTGGATAGGCC) with a thermal cycle: preheating by 95 °C for 2 min, 35 cycles of 95 °C for 30 s, 62.5 °C for 1 min, 72 °C for 2 min, followed by 72 °C for 5 min. PCR products were separated in 2% (wt/vol) agarose gel by electrophoresis and analyzed.

Video EEG and EKG. Mice were anesthetized with Avertin, and six cranial burr holes were created. Four silver-wire recording EEG leads were implanted bilaterally over frontal and posterior somatosensory cortex, and two reference electrodes were placed over the olfactory bulbs (1 mm rostral, 1 mm lateral from bregma). The electrocardiogram was recorded with a pair of leads sutured to the inner back muscles at the latissimus level. Mice were allowed to recover for at least 7 d after EEG surgery. EEG and EKG signals were acquired at 0.2 kHz and 2 kHz, respectively, and were amplified and analyzed using a Stellate Harmonie EEG system (Natus Medical Incorporated). Video was recorded throughout the monitoring. A cortical interictal spike was defined as sharp EEG deflection (>0.5 mV) appearing simultaneously in at least two EEG channels.

In Vitro Slice Electrophysiology. Slices were prepared as described previously (56). For genotype comparisons, slices from WT and mutant mice were prepared for study on the same day and pooled to conceal those carrying the mutant RQ allele. The genotypes were later unblinded by PCR methods (see *Animals*) after completion of the data analyses. Slices were transferred to the recording chamber (RC-27, Warner Instruments), superfused with artificial cerebrospinal fluid (ACSF; in mM: 126 NaCl, 3 KCl, 1.25 Na_2HPO_4, 26 $NaHCO_3$, 0.4 ascorbic acid, 10 glucose, equilibrated with 95% O_2/5% CO_2) at 3 mm/min and 33 °C.

SD thresholds were tested on randomly chosen slices prepared from WT and RQ mice on the same day. Slices were visualized with an upright microscope (BX51Wi, Olympus) equipped with a xenon light with differential inference contrast filters. SD was evoked by three different methods: For K-SD, a 1 M KCl microejection pipette was placed at the slice surface. The KCl microinjection was started with a 10-ms pulse (constant 40 psi), and the ejection duration was incrementally escalated up to 500 ms (10, 20, 50, 100, 300, and 500 ms) every 3 min. OGD–SD was induced by exposure to ACSF with reduced glucose (2 mM glucose/8 mM sucrose or 5 mM glucose/5 mM sucrose) and saturated by nitrogen (95% N_2/5% CO_2). In an experiment where SD was not detected within 22 min of the OGD challenge, data are presented as SD onset of 22 min and propagation of 0 mm/min. SD was also triggered by exposure to nominally Mg^{2+}-free ACSF (0 mM $MgSO_4$). Mg^{2+} removal evoked spontaneous spikes, seizure-like activities, and SD in the somatosensory cortical field (see Fig. 2*D*). In all experiments, SD was analyzed by DC electrical recordings with a glass microelectrode and/or bright field image acquired with a CCD camera (DMK22AU) at 1.0–0.2 Hz. SD was detected as a slowly traveling enhanced bright band (IOS). SD onset was determined by the first appearance of enhanced IOS signal in the imaging window, and propagation rate was calculated based on the distance of the IOS signal wave front from the initial site obtained from two to four consecutive images.

Whole-cell clamp recordings were made from visually identified pyramidal neurons in cortical layer II/III. Intrinsic excitability was characterized in current clamp using patch pipettes containing a potassium gluconate-based solution (in mM: 135 potassium gluconate, 10 Hepes, 8 sodium chloride, 0.05 EGTA, 2 ATP, 0.3 GTP, pH adjusted with potassium hydroxide). After bridge balance adjustment, membrane voltage was adjusted to ∼65 mV, and membrane properties were tested by injection of a test pulse (from –200 pA to 200 pA, 40 pA increments, 500 ms).

For voltage clamp recordings, pipettes were filled with a cesium-based internal solution [in mM: 115 cesium gluconate, 10 4-(2-hydroxyethyl)-1-piperazineethanesulfonic acid (Hepes), 10 1,2-bis(*o*-aminophenoxy)ethane-N,N,N′,N′-tetraacetic acid, 5 tetraethylammonium, 5 QX314, 2 ATP, 0.3 GTP, pH adjusted to 7.2 with cesium hydroxide). Recordings with a whole-cell capacitance within 80–150 pF and series resistance between 20 and 25 MΩ were analyzed. mEPSCs and mIPSCs were isolated by bath application of 1 μM tetrodotoxin (TTX) and sampled for >1,000 events (typically 3–5 min) at –70 mV and 10 mV, respectively, after a correction of 10 mV liquid junction potential. The mEPSCs and mIPSCs were analyzed using minianalysis software (Synaptosoft) with detection thresholds of 3 pA and 5 pA, respectively. For the analysis of mEPSC in dorsomotor vagal neurons, a 5-pA threshold was used. EPSCs were also evoked with a bipolar electrode (stimulus intensity ∼70% maximum) placed perpendicularly in the deep layer (V and VI) in the absence of any inhibitors. At least 10 traces were recorded from each cell, and the peak amplitude was used for analysis. No series resistance compensation was applied.

In Vivo Electrophysiology. Mice were anesthetized with urethane (1.5 mg/kg, intraperitoneal), and body temperature was maintained with a closed-loop heat blanket (Harvard Apparatus). Two skull areas (∼0.75 mm diameter, thinned until the lower cranial plate was visible) were created using a dental drill, and silver ball electrodes (0.5 mm diameter, spaced by 1 mm) were implanted and glued. A craniotomy (1 mm diameter) was made >1 mm caudal from the posterior recording electrode and covered with saline-soaked gelfoam until recordings began. Experiments were performed following the recovery of normal EEG activity. SD was elicited by topical application of a gelfoam pledget soaked with 0.5 M KCl at the craniotomy site, and recordings were made for 1 h. SD onset was determined as a DC deflection >–1 mV/min, and propagation rate was calculated based on the temporal difference of SD detection between the two recording electrodes. Propagation rate was calculated only for the first SD to avoid contamination by the run-down effect from repetitive tissue depolarization (57). Cortical EEG, EKG, brainstem DC, and respiratory signals were recorded as described previously (11). After recovery from surgery, mice showed heart rates >550 bpm and respiration rates between 1 and 2 Hz. Seizures were evoked by topical application of 4AP (100 mM) to the cranial window.

Drugs. TTX citrate salt was purchased from Tocris. TTX was dissolved in water, and a 10 mM stock solution was kept at –20 °C. Other reagents were also purchased from Sigma.

Statistics. Statistical tests were performed by nonparametric Mann–Whitney *U* test or Dunn's rank sum comparison, unless otherwise described in the text. Data are presented as means with standard deviation. Individual data points are displayed. A P value <0.05 was considered statistically significant.

ACKNOWLEDGMENTS. The R176Q/+ mice were kindly provided by Dr. Susan Hamilton (Baylor College of Medicine). This work was supported by NIH Center for SUDEP Research Grants NS090340 and NS29709 (to J.L.N.); NIH HL089598, HL091947, HL117641, and HL129570 (to X.H.T.W.); American Heart Association Grants 13EIA14560061 (to X.H.T.W.) and 14POST20130031 (to I.A.); and the Blue Bird Circle Foundation (J.L.N.).

1. Thurman DJ, Hesdorffer DC, French JA (2014) Sudden unexpected death in epilepsy: Assessing the public health burden. *Epilepsia* 55(10):1479–1485.
2. Ryvlin P, et al. (2013) Incidence and mechanisms of cardiorespiratory arrests in epilepsy monitoring units (MORTEMUS): A retrospective study. *Lancet Neurol* 12(10): 966–977.
3. Cole AJ, et al. (2013) Case records of the Massachusetts General Hospital. Case 18-2013: A 32-year-old woman with recurrent episodes of altered consciousness. *N Engl J Med* 368(24):2304–2312.
4. Glasscock E, Yoo JW, Chen TT, Klassen TL, Noebels JL (2010) Kv1.1 potassium channel deficiency reveals brain-driven cardiac dysfunction as a candidate mechanism for sudden unexplained death in epilepsy. *J Neurosci* 30(15):5167–5175.
5. Kalume F, et al. (2013) Sudden unexpected death in a mouse model of Dravet syndrome. *J Clin Invest* 123(4):1798–1808.
6. Goldman AM, et al. (2009) Arrhythmia in heart and brain: KCNQ1 mutations link epilepsy and sudden unexplained death. *Sci Transl Med* 1(2):2ra6.
7. Bagnall RD, et al. (2016) Exome-based analysis of cardiac arrhythmia, respiratory control, and epilepsy genes in sudden unexpected death in epilepsy. *Ann Neurol* 79(4):522–534.
8. Anderson JH, Bos JM, Cascino GD, Ackerman MJ (2014) Prevalence and spectrum of electroencephalogram-identified epileptiform activity among patients with long QT syndrome. *Heart Rhythm* 11(1):53–57.
9. Pietrobon D, Moskowitz MA (2014) Chaos and commotion in the wake of cortical spreading depression and spreading depolarizations. *Nat Rev Neurosci* 15(6):379–393.
10. Dreier JP (2011) The role of spreading depression, spreading depolarization and spreading ischemia in neurological disease. *Nat Med* 17(4):439–447.
11. Aiba I, Noebels JL (2015) Spreading depolarization in the brainstem mediates sudden cardiorespiratory arrest in mouse SUDEP models. *Sci Transl Med* 7(282):282ra46.
12. Ophoff RA, et al. (1996) Familial hemiplegic migraine and episodic ataxia type-2 are caused by mutations in the Ca2+ channel gene CACNL1A4. *Cell* 87(3):543–552.
13. van den Maagdenberg AM, et al. (2004) A Cacna1a knockin migraine mouse model with increased susceptibility to cortical spreading depression. *Neuron* 41(5):701–710.
14. Eikermann-Haerter K, et al. (2009) Genetic and hormonal factors modulate spreading depression and transient hemiparesis in mouse models of familial hemiplegic migraine type 1. *J Clin Invest* 119(1):99–109.
15. Tottene A, et al. (2009) Enhanced excitatory transmission at cortical synapses as the basis for facilitated spreading depression in Ca(v)2.1 knockin migraine mice. *Neuron* 61(5):762–773.
16. Ayata C, Shimizu-Sasamata M, Lo EH, Noebels JL, Moskowitz MA (2000) Impaired neurotransmitter release and elevated threshold for cortical spreading depression in mice with mutations in the alpha1A subunit of P/Q type calcium channels. *Neuroscience* 95(3):639–645.
17. Fill M, Copello JA (2002) Ryanodine receptor calcium release channels. *Physiol Rev* 82(4):893–922.
18. Priori SG, et al. (2001) Mutations in the cardiac ryanodine receptor gene (hRyR2) underlie catecholaminergic polymorphic ventricular tachycardia. *Circulation* 103(2): 196–200.
19. Tang Y, Tian X, Wang R, Fill M, Chen SR (2012) Abnormal termination of Ca2+ release is a common defect of RyR2 mutations associated with cardiomyopathies. *Circ Res* 110(7):968–977.
20. Mathur N, et al. (2009) Sudden infant death syndrome in mice with an inherited mutation in RyR2. *Circ Arrhythm Electrophysiol* 2(6):677–685.
21. Kannankeril PJ, et al. (2006) Mice with the R176Q cardiac ryanodine receptor mutation exhibit catecholamine-induced ventricular tachycardia and cardiomyopathy. *Proc Natl Acad Sci USA* 103(32):12179–12184.
22. Postma AV, et al. (2005) Catecholaminergic polymorphic ventricular tachycardia: RYR2 mutations, bradycardia, and follow up of the patients. *J Med Genet* 42(11): 863–870.
23. Giannini G, Conti A, Mammarella S, Scrobogna M, Sorrentino V (1995) The ryanodine receptor/calcium channel genes are widely and differentially expressed in murine brain and peripheral tissues. *J Cell Biol* 128(5):893–904.
24. Simkus CR, Stricker C (2002) The contribution of intracellular calcium stores to mEPSCs recorded in layer II neurones of rat barrel cortex. *J Physiol* 545(Pt 2):521–535.
25. Llano I, et al. (2000) Presynaptic calcium stores underlie large-amplitude miniature IPSCs and spontaneous calcium transients. *Nat Neurosci* 3(12):1256–1265.
26. Smith AB, Cunnane TC (1996) Ryanodine-sensitive calcium stores involved in neurotransmitter release from sympathetic nerve terminals of the guinea-pig. *J Physiol* 497(Pt 3):657–664.
27. Johenning FW, et al. (2015) Ryanodine receptor activation induces long-term plasticity of spine calcium dynamics. *PLoS Biol* 13(6):e1002181.
28. Lehnart SE, et al. (2008) Leaky Ca2+ release channel/ryanodine receptor 2 causes seizures and sudden cardiac death in mice. *J Clin Invest* 118(6):2230–2245.
29. Klassen TL, et al. (2014) High-resolution molecular genomic autopsy reveals complex sudden unexpected death in epilepsy risk profile. *Epilepsia* 55(2):e6–e12.
30. Johnson JN, Tester DJ, Bass NE, Ackerman MJ (2010) Cardiac channel molecular autopsy for sudden unexpected death in epilepsy. *J Child Neurol* 25(7):916–921.
31. Bauce B, et al. (2002) Screening for ryanodine receptor type 2 mutations in families with effort-induced polymorphic ventricular arrhythmias and sudden death: Early diagnosis of asymptomatic carriers. *J Am Coll Cardiol* 40(2):341–349.
32. Gniel HM, Martin RL (2010) Changes in membrane potential and the intracellular calcium concentration during CSD and OGD in layer V and layer II/III mouse cortical neurons. *J Neurophysiol* 104(6):3203–3212.
33. Bodhinathan K, Kumar A, Foster TC (2010) Redox sensitive calcium stores underlie enhanced after hyperpolarization of aged neurons: Role for ryanodine receptor mediated calcium signaling. *J Neurophysiol* 104(5):2586–2593.
34. Venetucci L, Denegri M, Napolitano C, Priori SG (2012) Inherited calcium channelopathies in the pathophysiology of arrhythmias. *Nat Rev Cardiol* 9(10):561–575.
35. Lamberts RJ, et al. (2015) Sudden cardiac arrest in people with epilepsy in the community: Circumstances and risk factors. *Neurology* 85(3):212–218.
36. Bardai A, et al. (2012) Epilepsy is a risk factor for sudden cardiac arrest in the general population. *PLoS One* 7(8):e42749.
37. Lauritzen M, et al. (2011) Clinical relevance of cortical spreading depression in neurological disorders: Migraine, malignant stroke, subarachnoid and intracranial hemorrhage, and traumatic brain injury. *J Cereb Blood Flow Metab* 31(1):17–35.
38. Eikermann-Haerter K, et al. (2011) Enhanced subcortical spreading depression in familial hemiplegic migraine type 1 mutant mice. *J Neurosci* 31(15):5755–5763.
39. Jiang D, et al. (2005) Enhanced store overload-induced Ca2+ release and channel sensitivity to luminal Ca2+ activation are common defects of RyR2 mutations linked to ventricular tachycardia and sudden death. *Circ Res* 97(11):1173–1181.
40. Emptage NJ, Reid CA, Fine A (2001) Calcium stores in hippocampal synaptic boutons mediate short-term plasticity, store-operated Ca2+ entry, and spontaneous transmitter release. *Neuron* 29(1):197–208.
41. Rhyu IJ, Abbott LC, Walker DB, Sotelo C (1999) An ultrastructural study of granule cell/Purkinje cell synapses in tottering (tg/tg), leaner (tg(la)/tg(la)) and compound heterozygous tottering/leaner (tg/tg(la)) mice. *Neuroscience* 90(3):717–728.
42. Dilekoz E, et al. (2015) Migraine mutations impair hippocampal learning despite enhanced long-term potentiation. *J Neurosci* 35(8):3397–3402.
43. Adasme T, et al. (2011) Involvement of ryanodine receptors in neurotrophin-induced hippocampal synaptic plasticity and spatial memory formation. *Proc Natl Acad Sci USA* 108(7):3029–3034.
44. Lee KF, Soares C, Thivierge JP, Béïque JC (2016) Correlated synaptic inputs drive dendritic calcium amplification and cooperative plasticity during clustered synapse development. *Neuron* 89(4):784–799.
45. Seidel JL, Escartin C, Ayata C, Bonvento G, Shuttleworth CW (2016) Multifaceted roles for astrocytes in spreading depolarization: A target for limiting spreading depolarization in acute brain injury? *Glia* 64(1):5–20.
46. Qin Z, et al. (2012) LIM domain only 4 (LMO4) regulates calcium-induced calcium release and synaptic plasticity in the hippocampus. *J Neurosci* 32(12):4271–4283.
47. Patel H, Shah P, Rampal U, Shamoon F, Tiyyagura S (2015) Arrythmogenic right ventricular dysplasia/cardiomyopathy (ARVD/C) and cathecholaminergic polymorphic ventricular tachycardia (CPVT): A phenotypic spectrum seen in same patient. *J Electrocardiol* 48(5):874–878.
48. Egan KR, Ralphe JC, Weinhaus L, Maginot KR (2013) Just sinus bradycardia or something more serious? *Case Rep Pediatr* 2013:736164.
49. Sumitomo N, et al. (2003) Catecholaminergic polymorphic ventricular tachycardia: Electrocardiographic characteristics and optimal therapeutic strategies to prevent sudden death. *Heart* 89(1):66–70.
50. Leenhardt A, et al. (1995) Catecholaminergic polymorphic ventricular tachycardia in children. A 7-year follow-up of 21 patients. *Circulation* 91(5):1512–1519.
51. Watanabe E, et al. (2014) Sudden cardiac arrest recorded during Holter monitoring: Prevalence, antecedent electrical events, and outcomes. *Heart Rhythm* 11(8): 1418–1425.
52. Faggioni M, et al. (2013) Accelerated sinus rhythm prevents catecholaminergic polymorphic ventricular tachycardia in mice and in patients. *Circ Res* 112(4):689–697.
53. Sah P, McLachlan EM (1991) Ca(2+)-activated K+ currents underlying the afterhyperpolarization in guinea pig vagal neurons: A role for Ca(2+)-activated Ca2+ release. *Neuron* 7(2):257–264.
54. Rogers RC, Nasse JS, Hermann GE (2006) Live-cell imaging methods for the study of vagal afferents within the nucleus of the solitary tract. *J Neurosci Methods* 150(1): 47–58.
55. Bennett HJ, Semba K (1998) Immunohistochemical localization of caffeine-induced c-Fos protein expression in the rat brain. *J Comp Neurol* 401(1):89–108.
56. Aiba I, Shuttleworth CW (2012) Sustained NMDA receptor activation by spreading depolarizations can initiate excitotoxic injury in metabolically compromised neurons. *J Physiol* 590(22):5877–5893.
57. Ayata C (2013) Pearls and pitfalls in experimental models of spreading depression. *Cephalalgia* 33(8):604–613.